J Neurophysiol
88: 2224–2231, 2002; 10.1152/jn.00739.2001.

Direction-Selective Neurons in the Optokinetic System With Long-Lasting After-Responses

NICHOLAS S. C. PRICE AND MICHAEL R. IBBOTSON
Visual Sciences, Research School of Biological Sciences, Australian National University, Canberra, ACT 2601, Australia

Received 4 September 2001; accepted in final form 1 July 2002

Price, Nicholas S. C., and Michael R. Ibbotson. Direction-selective neurons in the optokinetic system with long-lasting after-responses. *J Neurophysiol* 88: 2224–2231, 2002; 10.1152/jn.00739.2001. We describe the responses during and after motion of *slow* cells, which are a class of direction-selective neurons in the pretectal nucleus of the optic tract (NOT) of the wallaby. Neurons in the NOT respond to optic flow generated by head movements and drive compensatory optokinetic eye movements. Motion in the preferred direction produces increased firing rates in the cells, whereas motion in the opposite direction inhibits their high spontaneous activities. Neurons were stimulated with moving spatial sinusoidal gratings through a range of temporal and spatial frequencies. The slow cells were maximally stimulated at temporal frequencies <1 Hz and spatial frequencies of 0.13–1 cpd. During motion, the responses oscillate at the fundamental temporal frequency of the grating but not at higher-order harmonics. There is prolonged excitation after preferred direction motion and prolonged inhibition after anti-preferred direction motion, which are referred to as same-sign after-responses (SSARs). This is the first time that the response properties of neurons with SSARs have been reported and modeled in detail for neurons in the NOT. Slow cell responses during and after motion are modeled using an array of Reichardt-type motion detectors that include band-pass temporal prefilters. The oscillatory behavior during motion and the SSARs can be simulated accurately with the model by manipulating time constants associated with temporal filtering in the prefilters and motion detectors. The SSARs of slow cells are compared with those of previously described direction-selective neurons, which usually show transient inhibition or excitation after preferred or anti-preferred direction motion, respectively. Possible functional roles for slow cells are discussed in the context of eye movement control.

INTRODUCTION

Direction-selective visual neurons have been identified in every normally functioning visual system studied (e.g., frog retina: Lettvin et al. 1959; rabbit retina: Barlow et al. 1964; cat cortex: Hubel and Wiesel 1962; insect visual system: Hausen 1976). Direction-selective neurons typically increase their firing rates during motion in one preferred direction and either do not respond or have their spontaneous activities inhibited by motion in the opposite anti-preferred direction. In most cases, experimenters have concentrated on the responses during the period of motion stimulation. Barlow and Hill (1963) were the first to comment on cell firing in direction-selective cells after motion cessation, referred to here as after-responses. They revealed that in rabbit retinal ganglion cells, firing rates were transiently driven below the spontaneous activity immediately after motion in the preferred direction and increased slightly above the spontaneous activity following motion in the anti-preferred direction. Such responses are referred to here as opposite-sign after-responses (OSAR). OSARs have been linked to the psychophysical phenomena of the motion aftereffect (e.g., Barlow and Hill 1963; Hammond et al. 1988) and have been reported in the direction-selective neurons of many mammals (e.g., cat: Hammond et al. 1988; monkey: Petersen et al. 1985; wallaby: Ibbotson et al. 1998).

Here, we report on the response properties and after-responses of a class of direction-selective neurons (*slow* cells) in the pretectal nucleus of the optic tract (NOT) of the wallaby (Ibbotson et al. 1994). Neurons in the NOT are tuned to detect wide-field horizontal temporal-to-nasal motion over the contralateral eye (Collewijn 1975a; Ibbotson et al. 1994) and drive horizontal optokinetic responses that stabilize retinal images during head movements (Collewijn 1975b). Slow cells are maximally stimulated by low image velocities of less than 4°/s (Ibbotson and Price 2001) and the majority have a same-sign after-response (SSAR). The SSAR takes the form of a prolonged excitation after preferred direction motion and a prolonged inhibition after anti-preferred direction motion. This paper provides the first comprehensive description of directional neurons in the NOT that have SSARs. Work in the rabbit inferior olive has demonstrated a similar response after motion cessation termed a "carryover effect" (Arts et al. 2000). These directional cells prefer speeds of ~0.5°/s (Simpson and Alley 1974), similar to slow cells in the NOT. Given that the inferior olive receives direct efferents from the NOT (Takeda and Maekawa 1976), the similarity in motion after-responses and preferred speeds in the two nuclei is of interest in establishing the origin of the effect. We compare the responses of slow cells with other neurons in the NOT that have OSARs and simulate the response properties of the slow cells using an array of Reichardt-type motion detectors (Ibbotson and Clifford 2001a,b). Possible roles for neurons with SSARs are discussed in the context of controlling stabilizing eye movements.

METHODS

Preparation and stimulation

Results are derived from 18 adult wallabies, *Macropus eugenii*. Experimental procedures were approved by the animal experimentation

Address for reprint requests: M. R. Ibbotson, Visual Sciences, Research School of Biological Sciences, Australian National University, P.O. Box 475, Canberra, ACT 2601, Australia (E-mail: ibbotson@rsbs.anu.edu.au).

committee of the Australian National University and follow the guidelines of the National Health and Medical Research Council (Australia). Anesthesiology and surgery have been described in detail previously (Ibbotson et al. 1998). In brief, animals were fully anesthetized and paralyzed during recording with a continuous intravenous infusion of 5.6 ml/h of Hartmann's lactate solution (with 1 mg $\cdot$ kg^{-1} $\cdot$ h^{-1} of pentobarbitone, 4.2 mg $\cdot$ kg^{-1} $\cdot$ h^{-1} of suxamethonium chloride) and were respired with a mixture of 75% N_2O-25% O_2. Tungsten-in-glass microelectrodes were advanced through the brain to the nucleus of the optic tract (NOT) (Ibbotson et al. 1994). The action potential waveforms from all recorded cells were analyzed to confirm that they had characteristics typical of the soma rather than the axon (Bishop 1964). Extracellular responses were amplified, passed through a window discriminator and fed into an A/D converter (sample rate 1 kHz: Metrabyte Das-20). The spike arrival times were stored for off-line analysis.

Achromatic sine-wave gratings were generated by a computer controlled video display driver (AT Vista: True Vision, Indianapolis, IN) and presented on a display monitor (refresh rate: 97.7 Hz; 512 × 480 pixels; 45 cd/m^2; CCID7551: Barco Industries, Kortrijk, Belgium). The gratings subtended 67° vertically by 90° horizontally and could be positioned anywhere within the animal's visual field and could be presented in any orientation or moving in any direction. To create spatial sinusoidal gratings, a sawtooth function with period matching the grating's desired spatial wavelength was drawn into video memory. Each ramp in the sawtooth ranged in value from 0 to 255 or 0 to 1,023, depending on the program used. We then placed a gamma corrected sinusoid with a resolution of 256 or 1,024 brightness levels into an output look-up table (LUT). The ramps subsampled the values of the sine wave grating in the LUT, so the video output was a series of repeated sinusoids. To move the gratings, the LUT was permuted at the monitors frame rate (for the program with 256 values) or at half the frame rate (for the program with 1,024 values). The minimum displacement was either 1/256 of a cycle per frame or 1/1024 of a cycle every other frame. These programs allowed stimuli to be moved at temporal frequencies between 0.048 and 24.4 Hz. Previous experiments have revealed that the minimum integration time for the cells in the NOT is between approximately 20 and 40 ms (Ibbotson and Mark 1996). For the slowest moving pattern described in the preceding text, each frame was refreshed every 20.47 ms (2 frames), which is lower than the integration times for most cells.

Modeling

An array of 15 or 16 Reichardt-type elementary motion detectors (EMDs) was used to simulate the responses of the neurons (Reichardt 1961). The separation between the inputs of the detectors was 4 pixels and the array was 50 pixels in width (Fig. 1). Each detector had two subunits with opposite preferred directions, which consisted of four sequential stages: prefiltering, delay filtering, multiplication and summation. *Stage 1* (prefiltering): the image is operated on at all points by causal temporal filters with transient responses to changes in image intensity. The transient responses are achieved by subtracting the responses of a pair of first-order low-pass filters with different time constants (*Eq. 1*: τ_{Pre0} and τ_{Pre1}, where $\tau_{\mathrm{Pre0}} < \tau_{\mathrm{Pre1}}$). The gains of the two filters were adjusted using the prefilter gain, K, which has a value of 0–1

$$h(t) = \begin{cases} \left(\frac{1}{\tau_{\mathrm{Pre0}}}\right)\exp\left(\frac{-t}{\tau_{\mathrm{Pre0}}}\right) - \left(\frac{K}{\tau_{\mathrm{Pre1}}}\right)\exp\left(\frac{-t}{\tau_{\mathrm{Pre1}}}\right) & t \le 0 \\ 0 & t > 0 \end{cases} \quad (1)$$

If $K = 1$, the gains of the two low-pass filters are the same, thus their sustained responses to a fixed luminance cancel each other on subtraction. In this case, the resultant difference filter has a biphasic impulse response and a band-pass frequency response. For $0 < K < 1$, the temporal prefilter becomes low-pass and a scaled representation of the tonic luminance is seen at the prefilter's output. Because the size of steady-state oscillations at the fundamental frequency of the stimulus in the output of a single EMD is dependent on the tonic illumination, these oscillations only appear if $K < 1$ (Table 1).

The prefilter output from a given location was delayed by a temporal low-pass filter (*stage 2*: delay filtering) and multiplied (*stage 3*: multiplication) with the undelayed signal from the detector's other input channel. The temporal displacement between the signals is determined by the time constant (τ_{del}) of the delay filter. The two subunits that make up an EMD are tuned for motion in opposite directions. In *stage 4* (summation), the output from one subunit is subtracted from the output of the other to give the final response of the EMD (Fig. 1). If the opponent combination is unbalanced, some motion-independent signals are transmitted. We quantify the balance, β, of a motion detector according to the equation: $R(t) = P(t) - \beta \cdot A(t)$, where $P(t)$ and $A(t)$ are the outputs of the subunits responsive to preferred and anti-preferred motion, respectively, $R(t)$ is the motion detector response and $0 \le \beta \le 1$. Like the prefilter gain K, the balance term has a significant influence on the oscillatory responses of the detectors (Table 1). Finally, in *stage 5*, the responses of the array of motion detectors are spatially pooled to represent the input to a wide-field neuron (Fig. 1). If the response of the motion-detector array is positive, the model will respond above its baseline level. If the array response is negative, the response level will be below the resting level. The filter time constants, balance, and prefilter gain were adjusted to provide the best match by eye between the model outputs and cell responses over a range of temporal frequencies. It was not practical to provide a measure of this match because of the range of stimulus conditions and preferred temporal frequencies.

The normalized, steady-state response of a single EMD to a moving sinusoid can be expressed as: $X_i(t) = A + B \cdot \cos(\omega t + \phi_i)$, where ω is the angular velocity, t is time, A is the mean intensity of the sinusoid, B is the sinusoid amplitude and ϕ_i is the relative spatial position of the ith EMD in an array. Thus the spatially summated response of an array of j equally spaced EMDs is given by: $Y(t) = \Sigma_{\forall i} X_i(t)$, where $i = [1,j]$. Assuming closely and regularly spaced EMDs (as in Fig. 1), this response can be approximated by

$$Y(t) = \int_a^b A + B\cos(\omega t + \phi)d\phi$$

where a and b are the relative positions of the first and last EMDs in the array. Thus

$$\begin{aligned} Y(t) &= A(b-a) + B[\sin(\omega t + b) - \sin(\omega t + a)] \\ &= A(b-a) + 2B\cos\left(\omega t + \frac{b+a}{2}\right)\sin\left(\frac{b-a}{2}\right) \quad (2) \end{aligned}$$

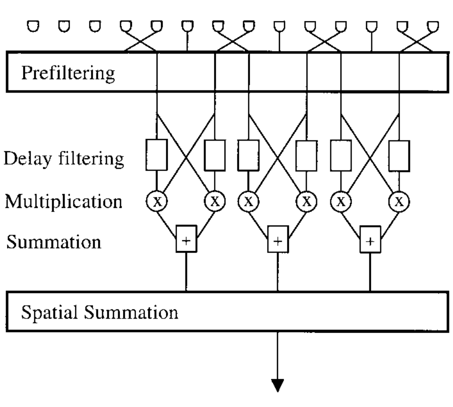

FIG. 1. Configuration of the motion detector array. The array has 5 serial stages: temporal prefiltering, delay filtering, multiplication, and summation occur within each elementary motion detector. The final stage is spatial summation of the outputs from all the elementary motion detectors. In the model, this comprised 15 or 16 EMDs spanning 50 input pixels.

TABLE 1. *Oscillations in the steady-state responses*

Model Parameters	Single EMD	EMD Array With Perfect Spatial Summation	EMD Array With Imperfect Spatial Summation
$\beta = 1; K = 1$	No oscillations	No oscillations	No oscillations
$\beta < 1; K = 1$	F_2	No oscillations	F_2 if $\beta \ll 1$
$\beta = 1; K < 1$	F_1	No oscillations	F_1 if $K \ll 1$
$\beta < 1; K < 1$	F_1 and F_2	No oscillations	F_1 and F_2

Oscillations in the steady-state responses of the model and their dependence on the prefilter gain, K, the elementary motion detector (EMD) balance, β, and the type of spatial summation. A definition of perfect and imperfect spatial summation is provided (see *Eq. 2*). F_1, F_2, oscillations at the fundamental and second harmonic of the stimulus frequency. The table should be compared with the simulations in Fig. 5.

When the first and last EMDs in the array are separated by an integer multiple k of the full period of the stimulus sinusoid we have $(b - a) = k2\pi$. This gives $Y(t) = A(b - a)$, which is a constant (*Eq. 2*), implying that no steady-state oscillations are present. This scenario is described as perfect spatial summation because individual motion detectors sample all phases of the stimulus equally. If $(b - a) \neq k2\pi$, there is an oscillatory component in $Y(t)$. This is described as imperfect spatial summation because the EMD array does not sample all points of the stimulus equally. This was achieved in the model by using $j = 15$ rather than 16 EMDs in the sampling array. If the stimulus covers only a portion of the motion detector array's "receptive field," imperfect spatial summation may occur because individual motion detectors cannot sample all phases of the sinusoidal grating.

RESULTS

Neuron classification

Recordings were made from direction-selective neurons in the pretectal NOT. Recording sites matched those used in previous studies of wallaby NOT (Ibbotson et al. 1994). Direction-selective responses were characterized by elevated firing rates relative to the spontaneous level during tempero-nasal motion over the contralateral eye (preferred motion) and reduced firing rates during naso-temporal motion (anti-preferred motion). All cells in the NOT had large receptive fields (≥40° in horizontal extent but usually much larger (>80°) and preferred wide-field stimuli. Previous investigations have shown that NOT neurons tested with sine-wave gratings moving in the preferred direction generate maximum responses at a particular combination of spatial and temporal frequencies (Ibbotson and Price 2001; Ibbotson et al. 1994). The spatiotemporal tuning shows that most cells are maximally responsive for a particular temporal frequency of motion across a range of spatial frequencies: temporal frequency selective neurons. A small percentage of cells (3%) respond with a similar firing rate for a given image velocity across a range of spatial frequencies: velocity-tuned cells. The neurons can be divided into two categories based on the location of the peak response in a spatiotemporal map (Ibbotson and Price 2001). Slow cells prefer low temporal frequencies (<1 Hz) and spatial frequencies of 0.13–1 cpd with a median preferred velocity of 0.79°/s (Ibbotson and Price 2001). *Fast* cells preferred higher temporal frequencies (0.4–20 Hz) and lower spatial frequencies (0.06–0.6cpd) with a median velocity of 50°/s. Another cell type, referred to as "jerk" (Schweigart and Hoffmann 1992) or SD cells (Price and Ibbotson 2001) is also known to exist in the NOT. The SD cells are nondirectional and are maximally stimulated by very rapidly moving images (>100°/s). We will not consider the SD cells in the present comparisons as they do not appear to be involved in the control of stabilizing eye movements.

Figure 2*A* shows typical peristimulus time histograms (PSTHs) from a fast cell stimulated with motion in preferred (*top*) and anti-preferred (*bottom*) directions. During motion, the response oscillates in phase with the moving grating. After the cessation of motion, the firing rate transiently decreases below the spontaneous level for preferred direction motion and increases above the spontaneous rate following anti-preferred direction motion (an OSAR). Neurons with these typical OSARs have been described frequently in the literature in a variety of species (see DISCUSSION). Figure 2*B* shows responses from a slow cell stimulated with motion in preferred and anti-preferred directions. After the cessation of motion, the responses slowly return to the spontaneous level over a period of several seconds, which we refer to as SSARs (Fig. 2*B*). The rest of the paper will focus on the response properties of 37 slow cells with SSARs.

Modeling the PSTHs of the slow cells

The responses of a slow cell to preferred-direction motion with a range of temporal frequencies are shown (Fig. 3*A*). For clarity, the responses were filtered with a Chebyshev-type I filter with a cutoff frequency 3.1 times the stimulus temporal frequency. This highlights the response oscillations at the stimulus frequency and does not attenuate any second har-

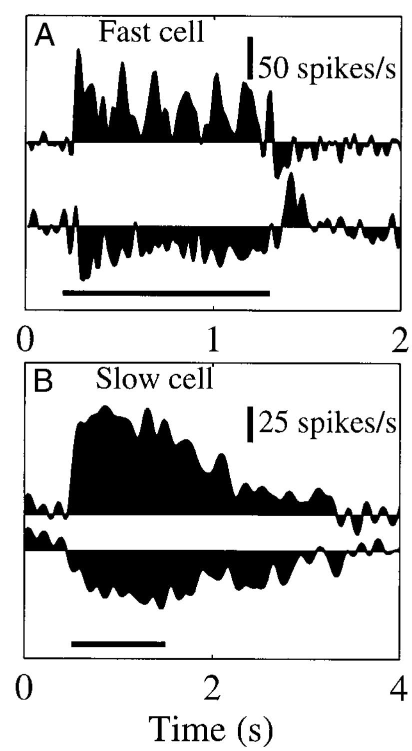

FIG. 2. *A*: peristimulus time histograms (PSTHs) derived during preferred (*top*) and anti-preferred (*bottom*) direction motion for a *fast* cell. The spontaneous firing rate was 60 spikes/s. *B*: PSTHs derived during preferred and anti-preferred direction motion for a slow cell. The spontaneous firing rate was 90 spikes/s. Horizontal bars show the period of motion. The grating moved at a temporal frequency of 6.4 Hz (0.2 cpd) for the fast cell and 0.38 Hz (1 cpd) for the slow cell. Contrast was 60% in both cases.

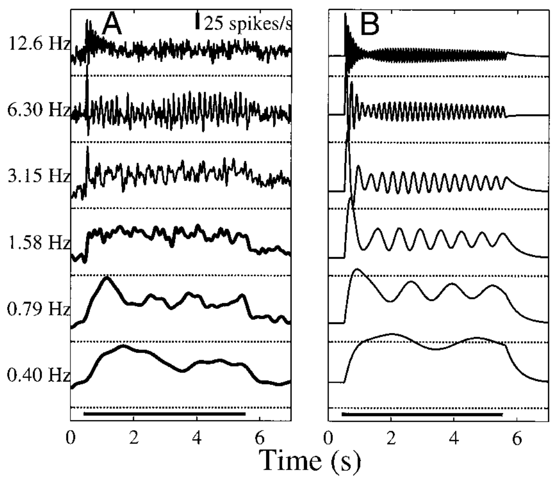

FIG. 3. Comparison of the responses of a slow cell and the model. *A*: slow cell responses to 5 s of grating motion in the preferred direction with temporal frequencies of 0.4–12.6 Hz (0.8 cpd). The mean spiking rate was 34 spikes/s. *B*: best fits of the model to the slow cell responses. Model parameters were: $\tau_{\mathrm{Pre0}} = 20$ ms; $\tau_{\mathrm{Pre1}} = 5{,}000$ ms; $\tau_{\mathrm{del}} = 400$ ms; $K = 0.85$; $\beta = 1$. In all plots, the dotted line marks the 0 spiking level.

monic response components. The responses shown are typical of the slow cells but some variations in the shapes of the PSTHs did occur between neurons. For example, some neurons had larger onset transients than others and the peak-to-peak amplitudes of the oscillations were noticeably different between cells, possibly because different cells had different spatial summation properties (Zanker and Quenze 1993). All slow cells have four characteristic physiological properties. First, they have high spontaneous activities ranging from 40 to 105 spikes/s across the cell population (mean = 56 spikes/s). Second, they show a transient response to motion onset, which is typically larger in magnitude than the response to continued motion. The transient response can be seen as the elevated firing rate during the passage of the first cycle of the stimulus grating in Fig. 3*A* except at 1.58 Hz, where no onset transient occurred. The size of the transient response relative to the sustained response increases with increasing temporal frequency (Fig. 3*A*). Third, after motion ceases, there is a clear SSAR (Figs. 2*B* and 3*A*). The size and duration of the SSARs varied between slow cells. Cells with optimum speed tuning at the high end of the slow cell speed tuning range (close to 4°/s) had small SSARs, and the size of the SSARs increased as the optimum speed tuning decreased. The cell in Fig. 3 has a relatively small SSAR, but it is still clearly different to the OSARs observed in fast cells recorded in the same preparation. Finally, responses to motion always oscillate at the stimulus temporal frequency (Fig. 3*A*) with Fourier analysis showing that no higher frequency oscillations of any significant amplitude were observed in slow cells (Fig. 4).

The simulations in Figs. 3*B* were produced using the array of 16 Reichardt-type EMDs. They show the outputs of a single model that best match the cell responses across all temporal frequencies. Better fits to individual temporal frequencies were possible, but this was not the aim of the model. The preferred temporal frequency (TF) of the model was set at 0.4 Hz, corresponding to the temporal frequency producing the largest sustained responses in the cell. This frequency determined the delay filter time constant τ_{del} in the EMDs: $\tau_{\mathrm{del}} = 1/(2\pi.\ \mathrm{TF})$ (Borst and Bahde 1986). The response properties shown in Fig.

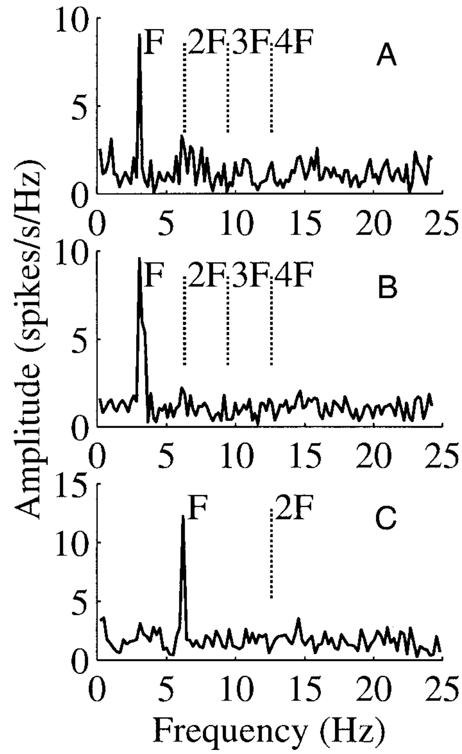

FIG. 4. *A–C*: Fourier transforms of the PSTHs of 3 slow cells. The positions of the fundamental (F) and harmonic frequencies (2F, 3F, etc) of the stimulus temporal frequency are marked (vertical dashed lines). All slow cells showed the general properties illustrated.

3*A* are reproduced by the model for temporal frequencies of 0.4–12.6 Hz (Fig. 3*B*). Oscillations at the fundamental frequency of the stimulus only occur in Reichardt detectors if several model parameters are set in specific ways (Table 1, Fig. 5). For a single EMD, oscillations at the fundamental frequency only occur if the prefilter gain, *K*, is <1. For second harmonic components to be present in addition to the fundamental, both *K* and the balance term, β, must be <1 (Fig. 5). As the slow cells only have oscillations at the fundamental

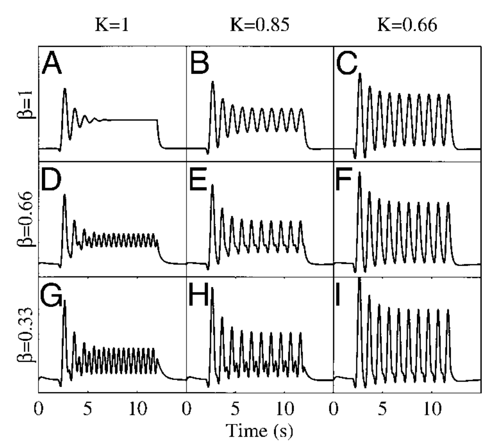

FIG. 5. Effects of varying the prefilter gain *K* and motion detector balance, β, on the oscillations in the responses of a single motion detector. The stimulus temporal frequency was 1 Hz. Oscillations in *B* and *C* are at the temporal frequency while in *G* they are at the 2nd harmonic of the stimulus frequency. The model parameters were: $\tau_{\mathrm{Pre0}} = 20$ ms; $\tau_{\mathrm{Pre1}} = 1{,}000$ ms; $\tau_{\mathrm{del}} = 200$ ms. Slow cell responses are most closely matched to *B*, which shows sustained oscillations at the stimulus temporal frequency and no 2nd harmonics.

frequency and the inhibition during anti-preferred motion is strong, we have modeled the results in Fig. 3 with $K = 0.85$ and $\beta = 1$. Importantly, an array of EMDs will not produce oscillations if all points of a sinusoidal grating are sampled equally (perfect spatial summation: *Eq. 2*). Oscillations will occur if the EMD array only samples part of the grating (imperfect spatial summation). Two potential sources of imperfect spatial summation in the physiological experiments were the size of the stimulus screen, which may have only covered part of each cell's receptive field, and a nonuniform distribution of EMDs, so that gaps or "hot spots" occurred in the coverage of the stimulus. A nonuniform distribution of EMDs could explain why oscillations at the fundamental frequency of the stimulus were observed in slow cell responses even when the stimuli subtended 90° horizontally.

Decay rate of SSARs

The decay time constant of the SSAR was determined for cells responding to motion in preferred and anti-preferred directions and for a range of stimulus durations. Figure 6*A* shows the PSTHs produced by 1–6 s of motion in preferred and anti-preferred directions for one slow cell. Responses to stimuli of the same duration have their spontaneous activities aligned, highlighting the symmetry of responses and after-responses to preferred and anti-preferred motion. Exponential fits to the SSARs are superimposed on each PSTH (thick lines). The time constants were calculated using a least-squares exponential fitting routine that used the cell's spontaneous firing level as an asymptote. The time constants of the exponential fits did not vary significantly with stimulus direction or duration. Plotted to the *right* of the neuron's responses are the outputs of the model (Fig. 6*B*). The model parameters in this case were: $\tau_{\mathrm{Pre0}} = 8$ ms, $\tau_{\mathrm{Pre1}} = 2{,}500$ ms, $\tau_{\mathrm{del}} = 2{,}500$ ms, $K = 1$, and $\beta = 1$. Calculating the preferred temporal frequency from τ_{del} gives a value of 0.064 Hz. The peak tuning for the neuron was 0.095 Hz, which is close to that of the model. It was not necessary to adjust K in these simulations because the stimulus duration was short relative to the temporal frequency, and thus oscillations were not clearly evident in the physiological data. It is clear from Fig. 6*B* that the decay rate of the SSAR in the model does not vary as the stimulus duration changes. As the balance, β, was unity, the responses to preferred and anti-preferred motion were identical in size but opposite in sign, which matches the neural responses.

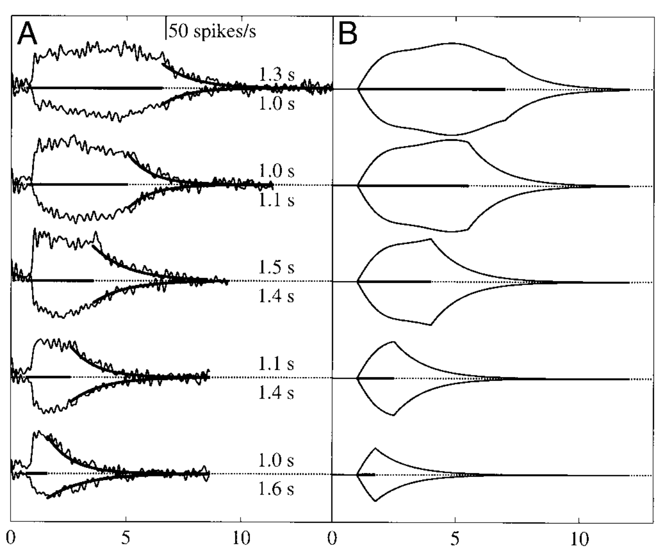

FIG. 6. Response decay after motion cessation. *A*: exponential fits (thick black lines) to the after-response decay of a slow cell following preferred (above dotted line) and anti-preferred (below dotted line) direction motion lasting 0.9–5.7 s. The fitted time constants are shown alongside each exponential in seconds. The mean spiking rate for the 10 responses shown was 100 ± 11 spikes/s. *B*: responses to preferred and anti-preferred direction motion produced by the model. The durations of motion are indicated by the thick horizontal lines, which in *A* also indicate the cell's spontaneous firing rate. Oscillations are not pronounced in these responses because the stimulus temporal frequency was 0.4 Hz (spatial frequency: 0.38 cpd).

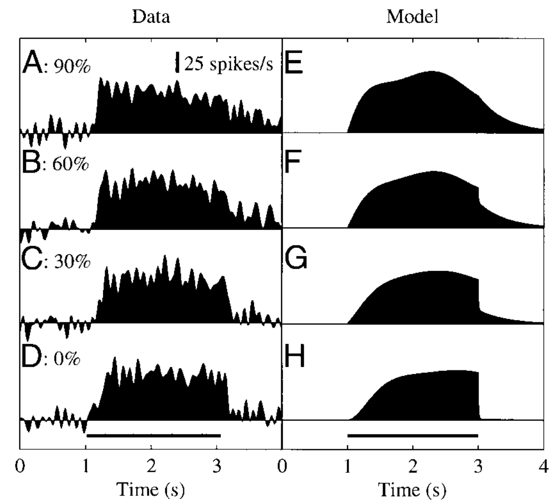

FIG. 7. *A–D*: PSTHs generated during motion stimulation in the preferred direction for a slow cell with mean spiking rate 51 spikes/s. The stimulus contrast of the moving stimulus is always 90% but varies in the stationary phases from 0 to 90%, as indicated. *E–H*: responses of the model to the same stimulus conditions in *A–D*. Horizontal bars show the 2 s period of motion with temporal frequency 0.4 Hz and spatial frequency 0.38 cpd.

Contrast dependence of after-responses

The shape of the after-responses of slow cells depends on the grating contrast after motion. Figure 7 shows the responses of a single slow cell to periods of grating motion preceded and followed by presentation of a stationary grating. In all cases, the contrast of the moving grating was held at 90% but the contrast of the stationary gratings were varied from 0 to 90%. With 0% contrast, the stationary stimulus is simply a blank gray screen. With no contrast change between the moving and stationary gratings, the response increases quite rapidly at motion onset but decays slowly after the period of motion, i.e., there is a clear SSAR (Fig. 7*A*). During the SSAR, the firing rate takes >1 s to return to the spontaneous level. With the maximum contrast change (i.e., 0–90%), the cell's firing rate increases more slowly after motion onset but the response drops off very quickly after the cessation of motion (Fig. 7*D*). Intermediate contrast changes show response properties between those described (Fig. 7, *B* and *C*). The output of the model shows similar properties (Fig. 7, *E–H*). The model parameters in this case were similar to those used previously: $\tau_{\mathrm{Pre0}} = 8$ ms, $\tau_{\mathrm{Pre1}} = 2{,}500$ ms, $\tau_{\mathrm{del}} = 500$ ms, $K = 1$, and $\beta = 1$. Again, it was not necessary to adjust K because the stimulus duration was short relative to the stimulus temporal frequency and thus oscillations are not evident. Most importantly, when there isn't a contrast change at motion onset and offset there is a rapid increase in response after motion starts and a slowly decaying SSAR following motion cessation (Fig. 7*E*). Conversely, with a large contrast change, the response increases slowly at motion onset but decays very rapidly at motion offset (Fig. 7*H*). This response pattern reflects that observed in the neuronal responses.

DISCUSSION

Slow cells have three physiological properties that will be discussed: they have high spontaneous firing rates; during stimulation with moving sinusoids the responses contain sustained oscillations at the fundamental frequency of the grating but not at higher frequencies; and the cells produce SSARs.

Spontaneous activity

The mean spontaneous activity for the slow cells was 56 spikes/s with several neurons having spontaneous rates close to 100 spikes/s. A high spontaneous rate allows a cell to effectively code two opposite directions of motion, thus halving the number of cells required to distinguish leftward from rightward motion. Direction-selective retinal ganglion cells and cortical units usually have low spontaneous activities (Barlow et al. 1964; Hubel and Wiesel 1962), so different cells are necessary to code different directions of motion.

The range of slow cell behavior is shown in Figs. 2*B* and 6. The inhibition during anti-preferred direction motion shown in Fig. 2*B* is approximately half the size of the excitation for preferred direction motion while the cell generating the responses in Fig. 6 produced equal sized inhibition and excitation for opposite motion directions. In the model, it is necessary to have $\beta < 1$ to simulate smaller inhibition for anti-preferred direction motion than excitation for preferred direction motion. However, if $\beta < 1$, the motion detectors produce response oscillations at the second harmonic of the input frequency (Fig. 5*G*), whereas slow cells produced no significant second harmonic components. We conclude that $\beta \cong 1$ in the motion detectors presynaptic to slow cells, so any differences in response sizes for opposite directions may result from response saturation, i.e., the membrane potential being driven below the spiking threshold during anti-preferred direction motion. Fast cells generate second harmonic components in their responses to moving sinusoidal gratings suggesting that in those neurons $\beta < 1$ (see Fig. 10*A* in Ibbotson et al. 1994). The inhibition produced during anti-preferred direction motion in fast cells is also typically smaller than the excitation produced by preferred direction motion, as expected if $\beta < 1$. Similarly, directional visual cells in insects produce second harmonic response components to moving sinusoids and the excitation during preferred direction motion is typically larger than the inhibition during anti-preferred motion (e.g., Egelhaaf et al. 1989; Ibbotson et al. 1991).

Response oscillations

To produce response oscillations from the model, it was necessary to have imperfect spatial summation of the EMD outputs. No oscillations occur in the output if the array contains uniformly distributed elementary motion detectors that sample all points of the stimulus equally (*Eq. 2*). For wide-field directional neurons in fly optic lobes, a moving sinusoid presented behind a narrow aperture oriented perpendicular to the cell's preferred direction of motion produces sustained oscillations (Egelhaaf et al. 1989; Zanker and Quenzer 1993). The aperture prevents spatial averaging of the inputs from the EMDs spread across the cell's receptive field. In contrast, wide-field stimulation of the same neurons doesn't produce oscillations in the responses, suggesting that perfect spatial summation occurs in the fly cells. In contrast, wide-field motion-sensitive cells in pigeon's display sustained oscillatory responses to stimuli with diameters of 120° (Wolf-Oberhollenzer and Kirschfeld 1994). Similarly, during prolonged stimulation, the slow cells in the wallaby oscillate at the fundamental frequency of the stimulus. These oscillations could arise if motion detectors were nonuniformly distributed, allowing imperfect spatial summation. Such a distribution may relate to a hot spot or region of dense EMDs or a patchy coverage of the visual scene by the EMDs.

When stimulated by moving sinusoidal gratings, slow cell responses oscillate at the fundamental frequency of the stimulus. These oscillations typically comprise two components: an initial component, which decays away in 1–3 s, and a steady-state oscillation of constant amplitude. Given imperfect spatial summation, oscillations at the fundamental frequency of the stimulus only arise if a DC-signal representing the mean stimulus intensity is passed by the prefilters (Ibbotson and Clifford 2001a,b; Ibbotson et al. 1991). When the prefilter gain is unity ($K = 1$), this cannot occur because the prefilter has band-pass frequency responses (*Eq. 1*). However, when $K < 1$, small mean luminance signals are passed by the prefilters, allowing the production of constant amplitude oscillations at the stimulus' fundamental frequency. The rate of decay of the transient oscillations is related to the decay time constants of the prefilters and delay filters in the motion detectors (Egelhaaf and Borst 1989). Thus these transient oscillations are present even when $K = 1$ and $\beta = 1$. It is unlikely that the oscillations observed in slow cell responses arise purely from a transient component because this would require excessively large filter time constants making motion detection unworkable. That is, the motion detectors would be optimally stimulated by very slow moving images that would not be behaviorally relevant.

SSARs

The fast cell responses exhibit the classical OSAR (Fig. 2*A*), which has been observed in directional neurons in many species (e.g., rabbit retina: Barlow and Hill 1963; cat cortex: Hammond et al. 1988; Maddess et al. 1988; insect optic lobes: Dürr and Egelhaaf 1999; Srinivasan and Dvorak 1979). Slow cells have after-responses where firing rates are sustained after motion stops at the same polarity as the response during motion (SSARs). Models incorporating arrays of EMDs of the Reichardt-type have been used to model motion detection in a range of species (beetle: Reichardt 1961; fly: Egelhaaf et al. 1989; butterfly: Ibbotson et al. 1991; pigeon: Wolf-Oberhollenzer and Kirschfeld 1994; wallaby: Clifford et al. 1997; Ibbotson et al. 1994, 1999). Computer models of biological motion detectors have not been able to account for the OSARs that follow motion cessation but instead show a SSAR in which the simulated firing rate decays exponentially from the response during motion to the spontaneous level (Egelhaaf et al.

1989). The slow cells show similar responses to those of correlation-type motion detectors. When modeling slow cell responses, τ_{Pre1} and τ_{del} control the decay rate of the SSAR. The other prefilter time constant, τ_{Pre2}, has little effect on the SSAR as it is very much smaller than the other time constants. The values of K and β have no effect on the SSAR.

What mechanisms could account for the different after-responses observed in fast and slow cells? One issue that could influence after-responses is the level of anesthesia. However, given that slow and fast cells are interspersed in the NOT and display same-sign and OSARs in the same preparation, different physiological mechanisms appear to provide a more likely explanation than the anesthetic state. Also, the duration and size of the SSAR could be manipulated by varying stimulus contrast, suggesting that the effect is related to visual stimulation. In other anesthetized preparations, SSARs have been observed but not discussed. For example Fig. 6 in Pereira et al. (1994) shows a slow increase in firing rate to the baseline level after a period of anti-preferred motion. In awake preparations, it is common to use adjacent periods of preferred and anti-preferred motion for NOT studies; something that conceals any motion after-responses, thus making comparisons with the present study difficult (e.g., Mustari and Fuchs 1990). However, in direction-selective neurons in area MT of the awake behaving monkey, approximately half of the neurons display excitatory after-responses (Droll et al. 2001). This after-response probably has a different origin to the after-responses observed in the NOT; however, it does demonstrate that after-responses have been observed in the absence of anesthesia.

Motion-sensitive neurons in the fly optic lobes accumulate calcium during motion stimulation (Borst and Egelhaaf 1992; Dürr and Egelhaaf 1999). The intracellular calcium concentration is velocity dependent and correlates with the after-hyperpolarization (OSAR) observed after motion in the preferred direction (Kurtz et al. 2000). Because calcium accumulation alone would depolarize the cells, Kurtz et al. (2000) proposed that the accumulated calcium opened calcium-sensitive potassium channels (K_{Ca} channels). This would facilitate rapid hyperpolarization when motion ceases because sodium influx associated with the motion response no longer depolarizes the cell. As calcium is sequestered or removed from the cell, the hyperpolarization facilitated by K_{Ca} channels would decrease, returning the membrane potential to its resting level. It is tempting to suggest that a similar mechanism is responsible for the OSAR in fast cells. Without K_{Ca} channels, it is expected that SSARs would occur as a consequence of the motion detector filters, as shown by our modeling.

Possible roles for slow cells

Slow cells in the wallaby are tuned to detect slow image velocities, with the median preferred velocity (temporal frequency/spatial frequency) being 0.79°/s (Ibbotson and Price 2001). Neurons in the NOT drive the ocular following phases of horizontal optokinetic nystagmus (OKN) that stabilize retinal images during head movements (e.g., Collewijn 1975a,b; Hoffmann et al. 1995). However, retinal slip velocities during head movements are rarely <1°/s in naturally behaving animals, even during stabilizing eye movements (Steinman and Collewijn 1980; Yakushin et al. 2000). Because most of the slow cells are maximally sensitive to wide-field retinal slip velocities ≤1°/s, they would not be optimally stimulated by the retinal slip during normal behavior. During fixation in rabbits (Collewijn and Van der Mark 1972), cats (Winterson and Robinson 1975), and primates (Steinman et al. 1973), the eyes are not perfectly stabilized and low-velocity (≤1°/s) eye movements occur. In fixating cats, "slow control" occurs where eye drift is counteracted by opposing eye movements (Winterson and Robinson 1975). Behavioral experiments show that wallabies actively fixate targets (Hemmi and Mark 1998), and it is plausible that slow cells help to stabilize eye position during fixation. Assisting fixation would complement the known function of the NOT in stabilizing the retinal image during head movements.

The vestibular apparatus generates a signal when the head is turned that drives counter-directed eye movements at a similar velocity to the head, interspersed with saccades that move in the same direction as the head (for review, see Buttner and Buttner-Ennever 1988). The characteristic saw-tooth pattern of eye position is referred to as vestibuloocular nystagmus (VOR). The VOR may not need to perfectly stabilize the retinal image during head movements because additional visual signals could be used to maintain good visual acuity (Collewijn 1989). For example, the NOT may play a role in bringing the gain of the VOR from values below unity to a level that is fully compensatory. That is, the slow cells, which are activated by slip speeds of <1°/s, could detect small differences between head and eye speed and supply signals that would move the eyes against the head direction more precisely. Interestingly, the optimal slip speeds for stimulating slow cells and modulating the floccular visual climbing fibers, which are thought to control the interaction between head movements and the VOR, are both 0.5–2°/s (Barmack and Hess 1980; Kusonoki et al. 1990; Simpson and Alley 1974). Further, the SSAR reported here has similar characteristics to the "carryover effect" reported in climbing fibers in the rabbit flocculus (Arts et al. 2000). As the NOT is known to provide a direct input to the inferior olive, it is possible that the carryover effect observed in the inferior olive has its origins in the NOT.

We thank Prof. Richard Mark and Dr. Lauren Marotte for help during experiments. Thanks are also due to Drs Clifford and Maddess for many helpful discussions and for reading and improving the manuscript.

N.S.C. Price was supported by a scholarship from the Australian National University.

REFERENCES

ARTS MP, DE ZEEUW CI, LIPS J, ROSBAK E, AND SIMPSON JI. Effects of nucleus prepositus hypoglossi lesions on visual climbing fiber activity in the rabbit flocculus. *J Neurophysiol* 84: 2552–2563, 2000.

BARLOW HB AND HILL RM. Evidence for a physiological explanation of the waterfall phenomenon and figural aftereffects. *Nature* 200: 1345–1347, 1963.

BARLOW HB, HILL RM, AND LEVICK WR. Retinal ganglion cells responding selectively to direction and speed of image motion in the rabbit. *J Physiol (Lond)* 173: 377–407, 1964.

BARMACK NH AND HESS DT. Multiple-unit activity evoked in the dorsal cap of inferior olive in the rabbit. *J Neurophysiol* 43: 151–163, 1980.

BISHOP PO. Properties of afferent synapses and sensory neurons in the lateral geniculate nucleus. *Int Rev Neurobiol* 6: 191–255, 1964.

BORST A AND BAHDE S. What kind of movement detector is triggering the landing response of the housefly? *Biol Cyber* 55: 59–69, 1986.

BORST A AND EGELHAAF M. In vivo imaging of calcium accumulation in fly interneurons as elicited by visual motion stimulation. *Proc Natl Acad Sci USA* 89: 4139–4143, 1992.

BUTTNER U AND BUTTNER-ENNEVER JA. Present concepts of oculomotor organization. In: *Neuroanatomy of the Oculomotor System,* edited by Buttner-Ennever JA. Amsterdam: Elsevier, 1988, p. 3–32.

CLIFFORD CWG, IBBOTSON MR, AND LANGLEY K. An adaptive Reichardt detector model of motion adaptation in insects and mammals. *Visual Neurosci* 14: 741–749, 1997.

COLLEWIJN H. Direction-selective units in the rabbit's nucleus of the optic tract. *Brain Res* 100: 489–508, 1975a.

COLLEWIJN H. Oculomotor areas in the rabbits midbrain and pretectum. *J Neurobiol* 6: 3–22, 1975b.

COLLEWIJN H. The vestibulo-ocular reflex: an outdated concept? *Prog Brain Res* 80: 197–209, 1989.

COLLEWIJN H AND VAN DER MARK F. Ocular stability in variable feedback conditions in the rabbit. *Brain Res* 36: 47–57, 1972.

DROLL JA, BISLEY JW, AND PASTERNAK T. The delay activity of some MT neurons may signal the remembered direction of motion (Abstract). *J Vision* 1: 20a, 2001.

DÜRR V AND EGELHAAF M. In *Vivo* calcium accumulation in presynaptic and postsynaptic dendrites of visual interneurons. *J Neurophysiol* 82: 3327–3338, 1999.

EGELHAAF M AND BORST A. Transient and steady-state response properties of movement detectors. *J Opt Soc Am A* 6: 116–127, 1989.

EGELHAAF M, BORST A, AND REICHARDT W. Computational structure of a biological motion detection system as revealed by local detector analysis. *J Opt Soc Am A* 6: 1070–1087, 1989.

HAMMOND P, MOUAT GSV, AND SMITH AT. Neural correlates of motion aftereffects in cat striate cortical neurones: monocular adaptation. *Exp Brain Res* 72: 1–20, 1988.

HAUSEN K. Functional characterization and anatomical identification of motion-sensitive neurons in the lobula plate of the blowfly *Calliphora erythrocephala. Z Naturforsch* 31: 629–633, 1976.

HEMMI JM AND MARK RF. Visual acuity, contrast sensitivity and retinal magnification in a marsupial, the tammar wallaby (*Macropus eugenii*). *J Comp Physiol [A]* 183: 379–87, 1988.

HOFFMANN K-P, DISTLER C, MARK RF, MAROTTE LR, HENRY GH, AND IBBOTSON MR. Neural and behavioral effects of early eye rotation on the optokinetic system in the wallaby *Macropus eugenii. J Neurophysiol* 73: 727–735, 1995.

HUBEL DH AND WIESEL TN. Receptive fields, binocular interaction and functional architecture in the cat's visual cortex. *J Physiol (Lond)* 160: 106–154, 1962.

IBBOTSON MR AND CLIFFORD CWG. Interactions between ON and OFF signals in directional motion detectors feeding the nucleus of the optic tract of the wallaby. *J Neurophysiol* 86: 997–915, 2001a.

IBBOTSON MR AND CLIFFORD CWG. Characterizing the temporal delay filters of biological motion detectors. *Vision Res* 41: 2311–2323, 2001b.

IBBOTSON MR, CLIFFORD CWG, AND MARK RF. Adaptation to visual motion in directional neurons of the nucleus of the optic tract. *J Neurophysiol* 79: 1481–1493, 1998.

IBBOTSON MR, CLIFFORD CWG, AND MARK RF. A quadratic non-linearity underlies direction selectivity in the nucleus of the optic tract. *Vis Neurosci* 16: 991–1000, 1999.

IBBOTSON MR, MADDESS T, AND DUBOIS R. A system of insect neurons sensitive to horizontal and vertical image motion connect the medulla and midbrain. *J Comp Physiol* 169: 355–367, 1991.

IBBOTSON MR AND MARK RF. Impulse responses distinguish two classes of directional motion-sensitive neurons in the nucleus of the optic tract. *J Neurophysiol* 75: 996–1007, 1996.

IBBOTSON MR, MARK RF, AND MADDESS TL. Spatiotemporal response characteristics of direction-selective neurons in the nucleus of the optic tract and dorsal terminal nucleus of the wallaby *Macropus eugenii. J Neurophysiol* 72: 2927–2943, 1994.

IBBOTSON MR AND PRICE NSC. Spatiotemporal tuning of directional neurons in mammalian and avian pretectum: a comparison of physiological properties. *J Neurophysiol* 86: 2621–2624, 2001.

KURTZ R, DURR V, AND EGELHAAF M. Dendritic calcium accumulation associated with direction-selective adaptation in visual motion-sensitive neurons *in vivo. J Neurophysiol* 84: 1914–1923, 2000.

KUSONKI M, KANO M, KANO MS, AND MAEKAWA K. Nature of optokinetic response and zonal organization of climbing fiber afferents in the vestibulocerebellum of the pigmented rabbit. I. The flocculus. *Exp Brain Res* 80: 225–237, 1990.

LETTVIN JY, MATURANA H, MCCULLOCH WS, AND PITTS WH. What the frog's eye tells the frog's brain. *Proc IRE* 47: 1940–1959, 1959.

MADDESS T, MCCOURT ME, BLAKESLEE B, AND CUNNINGHAM RB. Factors governing the adaptation of cells in area 17 of the cat cortex. *Biol Cybern* 59: 229–236, 1988.

MUSTARI MJ AND FUCHS AF. Discharge patterns of neurons in the pretectal nucleus of the optic tract (NOT) in the behaving primate. *J Neurophysiol* 64: 77–90, 1990.

PEREIRA A, VOLCHAN E, BERNARDES RF, AND ROCHA-MIRANDA CE. Binocularity in the nucleus of the optic tract of the opossum. *Exp Brain Res* 102: 327–338, 1994.

PETERSEN SE, BAKER JF, AND ALLMAN JM. Direction-specific adaptation in area MT of the owl monkey. *Brain Res* 346: 146–150, 1985.

PRICE NSC AND IBBOTSON MR. Pretectal neurons optimized for the detection of saccade-like movements of the visual image. *J Neurophysiol* 85: 1512–1521, 2001.

REICHARDT W. Autocorrelation, a principle for the evaluation of sensory information by the central nervous system. In: *Sensory Communication,* edited by Rosenblith WA. New York: Wiley, 1961, p. 303–317.

SCHWEIGART G AND HOFFMANN KP. Pretectal jerk neuron activity during saccadic eye movements and visual stimulations in the cat. *Exp Brain Res* 91: 273–283, 1992.

SIMPSON JI AND ALLEY KE. Visual climbing fiber input to rabbit vestibulocerebellum: a source of direction-specific information. *Brain Res* 82: 302–308, 1974.

SRINIVASAN MV AND DVORAK DR. The waterfall illusion in an insect visual system. *Vision Res* 19: 1435–1437, 1979.

STEINMAN RM AND COLLEWIJN H. Binocular retinal image motion during active head rotation. *Vision Res* 20: 415–429, 1980.

STEINMAN RM, HADDAD GM, SKAVENSKI AA, AND WYMAN D. Miniature eye movement. *Science* 181: 810–819, 1973.

TAKEDA T AND MAEKAWA K. The origin of the pretecto-olivary tract. A study using the horseradish peroxidase method. *Brain Res* 117: 319–325, 1976.

WINTERSON BJ AND ROBINSON DA. Fixation by the alert but solitary cat. *Vision Res* 15: 1349–1352, 1975.

WOLF-OBERHOLLENZER F AND KIRSCHFELD K. Motion sensitivity in the nucleus of the basal optic root of the pigeon. *J Neurophsyiol* 71: 1559–1573, 1994.

YAKUSHIN SB, GIZZI M, REISINE H, RAPHAN T, BUTTNER-ENNEVER J, AND COHEN B. Functions of the nucleus of the optic tract (NOT). II. Control of ocular pursuit. *Exp Brain Res* 131: 433–47, 2000.

ZANKER JM AND QUENZE T. Long-lasting oscillations in motion-sensitive neurons driven by movement of high-contrast gratings. *Naturwissenschaften* 80: 134–137, 1993.